

PCCP

Accepted Manuscript



This is an *Accepted Manuscript*, which has been through the Royal Society of Chemistry peer review process and has been accepted for publication.

Accepted Manuscripts are published online shortly after acceptance, before technical editing, formatting and proof reading. Using this free service, authors can make their results available to the community, in citable form, before we publish the edited article. We will replace this *Accepted Manuscript* with the edited and formatted *Advance Article* as soon as it is available.

You can find more information about *Accepted Manuscripts* in the [Information for Authors](#).

Please note that technical editing may introduce minor changes to the text and/or graphics, which may alter content. The journal's standard [Terms & Conditions](#) and the [Ethical guidelines](#) still apply. In no event shall the Royal Society of Chemistry be held responsible for any errors or omissions in this *Accepted Manuscript* or any consequences arising from the use of any information it contains.

Can We Judge an Oxide by its Cover? The Case of Platinum over α -Fe₂O₃ from First Principles

Ofer Neufeld¹ and Maytal Caspary Toroker^{2,*}

¹The Nancy and Stephen Grand Technion Energy Program and ²Department of Materials Science and Engineering, Technion - Israel Institute of Technology, Haifa 32000, Israel

Keywords: Water splitting, Density Functional Theory, DFT+U, Iron oxides, Metal/Metal-oxide Interface.

Abstract

Metal/metal-oxide interfaces appear in a wide variety of disciplines including electronics, corrosion, electrochemistry, and catalysis. Specifically, covering a metal-oxide with a metal is often thought to enhance solar energy absorption and to improve photocatalytic activity. For example, the platinum/hematite (Pt/ α -Fe₂O₃) interface has demonstrated improved functionality. In order to advance our understanding of how metal coverage over an oxide helps performance, we characterize the geometry and electronic structure of the Pt/ α -Fe₂O₃ interface. We investigate the interface using density functional theory +U, and find a stable crystallographic orientation relationship: Fe₂O₃(0001)[1 $\bar{1}$ 00]||Pt(111)[10 $\bar{1}$] that agrees with experiment. Furthermore, there are significant changes in the electronic structure of α -Fe₂O₃ as a result of Pt coverage. We therefore suggest the concept of “judging” the electronic properties of an oxide only with its cover. Specifically, covering Fe₂O₃ with Pt reduces carrier effective mass and creates a continuum of states in the band gap. The former could be beneficial for catalytic activity, while the latter may cause surface recombination. In order to circumvent this problem, we suggest putting metal coverage behind the oxide and far from the electrolyte in a photoelectrochemical device in order to quickly collect electron carriers and avoid recombination with vulnerable holes accumulating as a result of catalysis at the surface.

*Corresponding author: E-mail: maytalc@tx.technion.ac.il, Tel.: +972 4 8294298.

I. Introduction

Metal/metal-oxide interfaces are widely used in a variety of technological applications, such as sensors, electronic devices, catalysts and catalyst supports in various chemical reactions.¹⁻⁸ Some examples include water oxidation in photoelectrochemical (PEC) cells,⁹⁻¹³ water gas shift (WGS),¹⁴⁻¹⁶ selective carbon monoxide (CO) oxidation,^{6, 17-19} and H₂ oxidation in polymer electrolyte membrane fuel cells (PEMFC).²⁰⁻²³

One such metal-oxide is hematite (α -Fe₂O₃, α dropped from this point), a widely used water oxidation catalyst. Fe₂O₃ is used in PEC cells as a photoanode with benefits of being environmentally safe, abundant, inexpensive, having a narrow band gap of about 2 eV, and having an appropriate valence band edge position for water oxidation. However, Fe₂O₃ is limited by poor charge transport, high recombination rates, and a large overpotential.¹⁰ There are many strategies to deal with these limitations; among them is to cover Fe₂O₃ with platinum metal.

We now list several experimental evidences for improvement in Fe₂O₃ functionality by Pt coverage. First, Fe₂O₃@Pt core shell particles were recently seen to improve efficiency in PEMFC.²¹ Second, Pt supported on Fe₂O₃ was measured to have increased catalytic activity and selectivity in WGS reaction.¹⁴ Third, coating of Pt over Fe₂O₃ has been seen to enhance the photocatalytic activity of Fe₂O₃.²⁴ Pt can also be used as a reflecting layer to increase absorbance in Fe₂O₃.²⁵ Finally, Fe₂O₃ films modified by metallic nanoparticles such as gold can increase absorption in the oxide via the plasmonic effect.²⁶

All of these encourage better understanding of how metal coverage enhances catalytic activity in the Pt/Fe₂O₃ system. Thus, the goal of this research is to investigate geometric and electronic structure in the Pt/Fe₂O₃ interface and to determine the stability and potential catalytic properties of this system. This is the first theoretical study on Pt/Fe₂O₃ where: 1) we model different interface thicknesses, 2) account for different interface orientation relationships, 3) calculate the interfacial energy of adhesion, and 4) present an electronic structure study of the interface. We find that the carrier effective mass in the metal-oxide reduces upon metal coverage and suggest that this could be beneficial for catalytic activity.

II. Computational Details

Density Functional Theory:

All calculations were performed using the Vienna Ab Initio Simulation Package (VASP).²⁷⁻²⁹ We used the spin polarized density functional theory +U (DFT+U) formalism of Dudarev *et al.*³⁰ to better represent electronic interactions in Fe₂O₃.³¹⁻³³ A U value of 4.3 eV which was derived ab-initio³⁴ was chosen for the Fe atoms in order to correctly describe the Fe₂O₃ ground state.^{35, 36} No explicit orbital corrections were given to Pt and O atoms (that is, a U value of 0 was chosen) since these atoms do not have half-filled orbitals with highly correlated electrons as in Fe, and since Pt and Pt oxides are well described by regular DFT exchange correlation (XC) approximations.³⁷⁻⁴⁰

The XC functional used in all computations was the Perdew-Burke-Ernzerhof (PBE)⁴¹ of the general gradient approximation (GGA). This XC functional was chosen since it was shown previously to describe well systems of Fe₂O₃, Pt, and Pt oxides.^{12, 37-40} Projected augmented wave (PAW) potentials^{42, 43} replaced inner frozen core electrons and nuclei of each atom. For Fe, O, and Pt atoms the appropriate PAW potentials replaced the [Ar], [He], and [Xe]4f¹⁴ inner shell electrons, respectively, since these previously converged the electronic structure as well as the effective mass in Fe₂O₃ and Pt-doped Fe₂O₃.^{34, 40}

The Kohn-Sham equations were solved self-consistently in a plane-wave basis set with 3D periodic boundary conditions under a tolerance of 10^{-5} eV in total energy. Symmetry was not imposed in order to best describe the interface geometry. K-space integration took place using the tetrahedron method with Blöchl corrections.^{44, 45} Geometrical relaxations were performed with the conjugate gradient algorithm⁴⁶ and converged with a criteria of 0.03 eV/Å. In all slab calculations the slabs were separated from their periodic image by a 10 Å vacuum layer which converged the total energy to a tolerance of 0.1 meV/atom. Ionic charges were calculated using the Bader charge analysis.⁴⁷ In the supporting information, we provide the relaxed geometries as well as specify for each structure the k-grid and plane-wave energy cutoff that converged total energies <0.1 meV/atom.

Structural details:

Constructing the interface of Pt(111)/Fe₂O₃(0001) required initial calculations of the bulk materials as well as calculations of the individual Pt(111) and Fe₂O₃(0001) surface slabs that were cleaved from bulk unit cells. Below we show how we constructed these structures and the interface.

Bulk Fe₂O₃ calculations used the 30-atom hexagonal lattice with long range antiferromagnetic ordering,^{48, 49} relaxed in shape, volume, and atomic positions (Figure 1a). This bulk structure was cleaved in the (0001) surface with an oxygen-atom termination and a thickness of four stoichiometric units as seen in Figure 1b, marked slab 1 (“Fe₂O₃ S1”), containing 23 atoms. We performed a linear transformation of coordinates to obtain a supercell of 46 atoms with an orthorhombic lattice that is then cleaved in the (0001) surface with an oxygen-atom termination and thickness of four stoichiometric units, marked slab 2 (“Fe₂O₃ S2”) and seen in Figure 1c. The Fe₂O₃ S1 and S2 slabs were later used to construct two different interface orientation relationships.

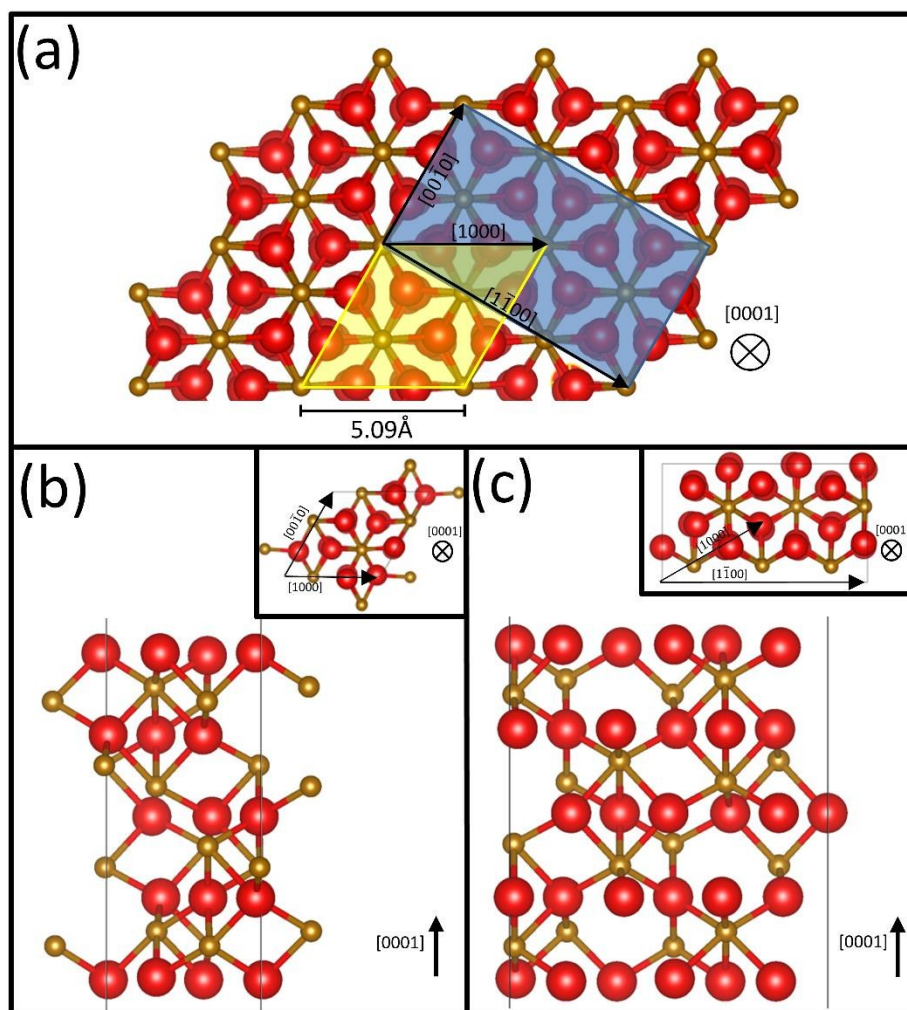


Figure 1 – Unit cells of Fe₂O₃: (a) Bulk Fe₂O₃ in hexagonal structure facing the [0001] direction, (b) the Fe₂O₃ S1 cell, and (c) the Fe₂O₃ S2 cell. Yellow and blue shaded areas in (a) are the cleavage planes for the Fe₂O₃ S1 and S2 cells as shown in the insets of (b) and (c), respectively. Atom colors red and gold represent O and Fe atoms, respectively. Created with VESTA.⁵⁰

Pure Pt was modeled with the four-atom face centered cubic (FCC) cell,³⁸ relaxed in shape, volume, and atomic positions, as seen in Figure 2a. This bulk structure was linearly transformed such that the (111) surface is in the z direction and the supercell contains three Pt atoms. This bulk structure was used to build two Pt(111) slabs: a hexagonal slab marked “Pt S1”, and another orthorhombic slab marked “Pt S2”, as seen in Figures 2b and 2c, respectively (the notations for the slabs of Fe₂O₃ and Pt are similar since, for example, the “Fe₂O₃ S1” and “Pt S1” will form the “S1 interface”). Pt S1 contains four Pt atoms per (111) atomic layer and Pt S2 contains six Pt atoms per (111) atomic layer.

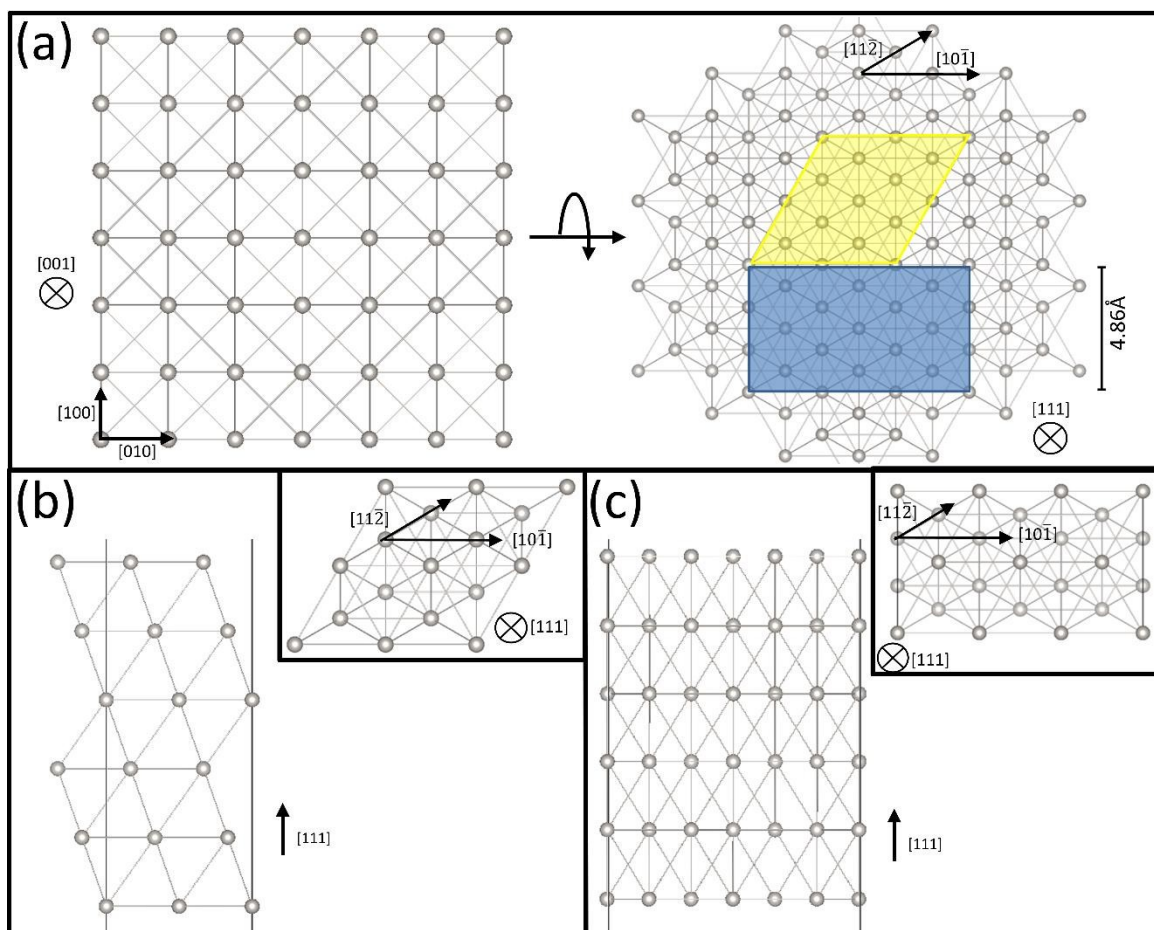


Figure 2 – Unit cells of Pt: (a) Bulk Pt in FCC structure facing [001] (left) and [111] (right) directions. (b) Pt S1 cell, and (c) Pt S2 cell. In yellow and blue shaded areas in (a) are the cleavage planes for the Pt S1 and S2 cells, respectively. Atom color gray represents Pt atoms. Created with VESTA.⁵⁰

We consider the oxygen-terminated (0001) slab of hematite for several reasons. First, this termination is known to be one of the more stable terminations of Fe_2O_3 ,⁵¹⁻⁵⁴ where we can compare our results to previous work.^{12, 40, 53, 55} In addition, we know there should be strong bonding between the negatively charged O ions and positively charged Pt ions at the interface, which would result in this termination being highly stable, more so than the Fe-terminated Fe_2O_3 . This is supported by a previous DFT study on Au and Pd adatoms which adsorbed more strongly to O terminated $\text{Fe}_2\text{O}_3(0001)$.⁵¹ Also, previous DFT calculations found this termination stable in a similar interface of $\text{Pt}(111)/\text{Al}_2\text{O}_3(0001)$, consistent with experiment in $\text{Pt}(111)/\text{Al}_2\text{O}_3(0001)$.⁵⁶ A final point is that since the (0001) and (111) planes of Fe_2O_3 and Pt, respectively, both have hexagonal symmetry, they can be arranged to build a smooth epitaxial interface with relatively low miss-fit.

Two interfaces were constructed: an “S1 interface” with an orientation relationship of $\text{Fe}_2\text{O}_3(0001)[1000]||\text{Pt}(111)[10\bar{1}]$ contains four stoichiometric units of Fe_2O_3 with an oxygen terminated (0001) surface and layers of Pt (111) planes appear on both sides in order to avoid forming a dipole across the unit cell, as seen in Figures 3a and 3b. An “S2 interface” with an orientation relationship of $\text{Fe}_2\text{O}_3(0001)[1\bar{1}00]||\text{Pt}(111)[10\bar{1}]$ contains four stoichiometric units of Fe_2O_3 with an oxygen terminated (0001) surface and layers of Pt (111) planes appear on both sides, as seen in Figures 3c and 3d. Both interfaces were relaxed in atomic positions and relative translations of the two materials.

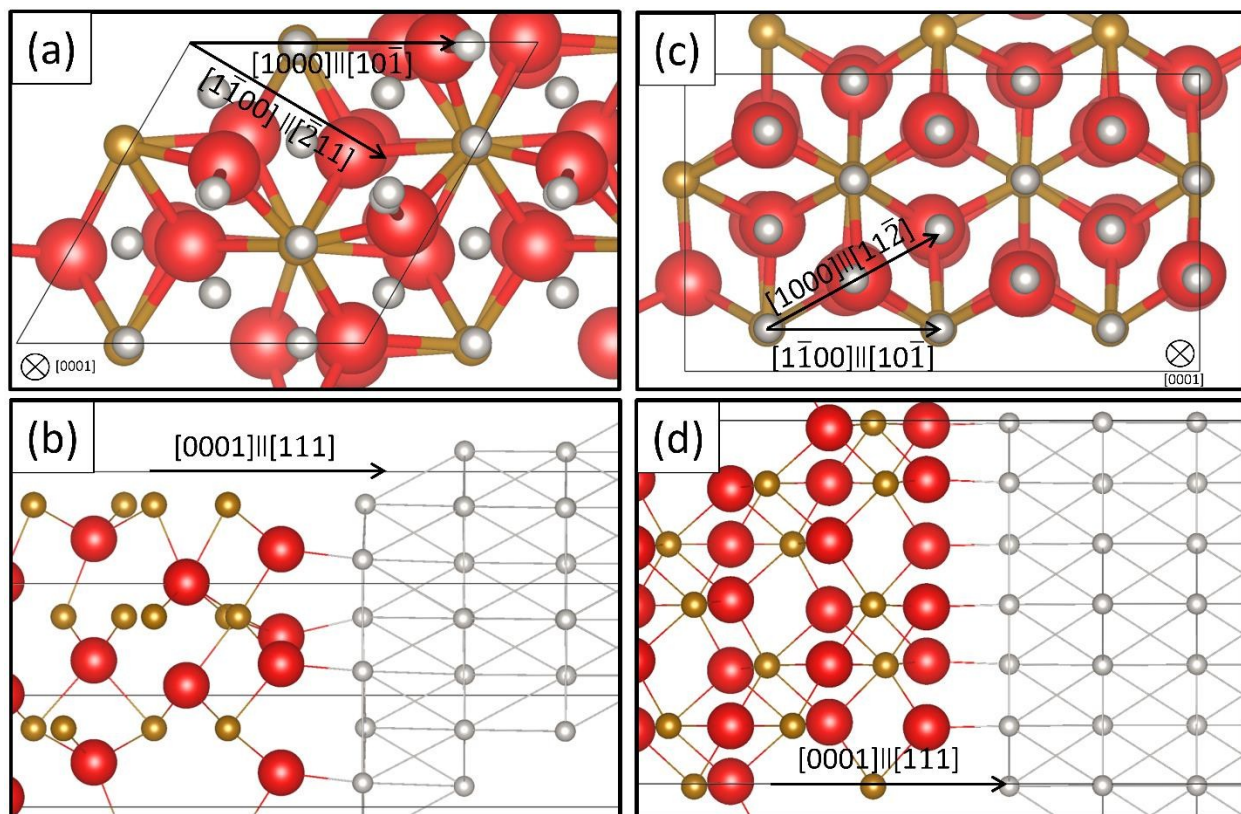


Figure 3 – Unit cells of the Pt/Fe₂O₃ interface: (a) S1 relaxed interface viewed from [111],[0001] directions of Pt and Fe₂O₃, respectively. (b) S1 relaxed interface, side view. (c) S2 relaxed interface viewed from [111],[0001] directions of Pt and Fe₂O₃, respectively. (d) S2 relaxed interface, side view. Atom colors red, gold, and grey correspond to O, Fe, and Pt atoms, respectively. Created with VESTA.⁵⁰

Miss-Fit:

The miss-fit m_{12} of lattice parameters of “material 1” relative to “material 2” is defined as⁵⁷⁻⁵⁹:

$$(1) m_{12} = \frac{a_1 - a_2}{a_2}$$

where a_1 and a_2 are slab lattice constants of “material 1” and “material 2”, respectively. An algorithm exists to minimize this miss-fit by increasing the size of the supercell through multiplication of a_1 and a_2 by integers until a minimum is reached, and doing this for every possible rotation of the interface.^{57, 59} In our case a minimum in the misfit is reached in non-feasible supercell sizes (>1000 atoms). The possible slabs with a minimal misfit and a feasible system size are the S1 and S2 interface slabs defined above.

To deal with the miss-fit of these interfaces we use the following algorithm: we perform calculations of total energy while relaxing ionic positions and constraining the lattice shape and vector lengths to a parameter in the range: $\alpha \in [a_1, a_2]$. We calculate the total energy of the interface for a set of α values. We then minimize the total energy per α , as suggested in ref. 60, but in addition, we choose α according to the following criterion:

We choose slabs with the inner (non-interface) layers of Pt and Fe₂O₃ that appear with a bulk-like structure after relaxation, such that atomic symmetry, coordination numbers, and bond distances remain intact and relatively close to those in the bulk materials (with a distortion smaller than the miss-fit).

Without this criterion the α of the S2 interface does not change, while the α of the S1 interface differs by 0.1 Å, the interface total energy differs by 0.6 eV, and the adhesion energy differs by 0.2 J/m².

With this algorithm we find an optimal lattice vector length, α , for the S1 and S2 interfaces. We find for the S1 interface: $a_1=b_1=5.36$ Å, $\alpha_1=\beta_1=90^\circ$, $\gamma_1=60^\circ$, with 4.7% miss-fit on Pt and 5.1% miss-fit on Fe₂O₃ in both a_1 and b_1 lattice parameters. For the S2 interface we find: $a_2=8.63$ Å, $b_2=4.98$ Å, $\alpha_2=\beta_2=\gamma_2=90^\circ$, with 2.25% miss-fit on Pt and Fe₂O₃ for the a_2 lattice parameter, and 2.3% and 2.25% miss-fit on Fe₂O₃ and Pt respectively for the b_2 lattice parameter. All relaxed structures for the pure materials (bulk and slabs) and the interfaces can be found in the supporting information.

Interface Energy of Adhesion:

The interface energy of adhesion (IEA) was calculated according to:⁵⁸⁻⁶⁰

$$(2) \gamma_{adh} = \frac{(2\varepsilon_{Pt} + \varepsilon_{Fe_2O_3}) - \varepsilon_{Pt/Fe_2O_3}}{2A_{int}}$$

where ε_i is the total energy of slab “i” with lattice vectors of the bulk “i” material that has a similar number of atomic layers as in ε_{Pt/Fe_2O_3} . ε_{Pt/Fe_2O_3} is the energy of the relaxed interface with the optimal α parameter. A_{int} is the area of the interface. This formula measures the preference for forming an interface.

The IEA was converged up to 0.08 J/m² with a four stoichiometric unit thick layer of Fe₂O₃ (for the S1 interface with four Pt layers). In the S2 interface, the IEA was converged up to 0.05 J/m² with six Pt layers. Overall, this converged the IEA of the S2 interface by 0.1 J/m². In S1 we encountered convergence difficulties with respect to number of Pt layers. This slow convergence arises from the large miss-fit in the S1 interface. Changing the lattice vectors from the ideal “ α ” to the Pt bulk parameters may speed up convergence, however, there will be large strains in Fe₂O₃ (an increase of 0.5 Å in Fe-O bond length). Nevertheless, with the ideal “ α ” the S1 interface geometry remains stable (<0.03 Å changes in Pt-O distances) with addition of Pt layers. Furthermore, as specified in the results, the S1 interface is inherently less stable, with a lower IEA than the S2 interface at the same number of Pt layers.

Valence band edge position:

We calculated the valence band edge position relative to vacuum for the pure slabs of Pt(111) and Fe₂O₃(0001), respectively. This was performed by aligning the energy of the last occupied orbital relative to the potential energy in the vacuum region.^{61, 62}

Charge transfer calculation:

We calculate a charge of valence electrons located in a region of space by integrating the self-consistent charge density directly over that region, such that for instance, the number of electrons in a volume Ω can be found by:

$$(3) N_{\Omega} = \int_{\Omega} \rho(\vec{x}) d\Omega$$

Effective mass:

Effective carrier mass was calculated from the density of states (DOS). The conduction band DOS curve can be approximated with a 3D isotropic, parabolic, band approximation.^{63, 64}

$$(4) g_{elec}(E) = \xi_{spin} \frac{V}{2\pi^2} \left(\frac{2m_e^*}{\hbar^2} \right)^{3/2} \sqrt{E - E_g}$$

where ξ_{spin} is the spin degeneracy factor, V is the volume of the oxide, E_g is the band gap, \hbar is the reduced Planck's constant, and m_e^* is the effective electron mass. This approximation correlates the DOS and effective mass such that the more abrupt and sharp the DOS conduction band peak is, the higher the effective state's mass (by power law of 2/3 as seen in Eq.4). We use this correlation to approximate the change in effective mass in the oxide under metal coverage, a more specific explanation can be found in the appendix A.1.

Metal/metal-oxide interface Schottky barrier:

In order to characterize the interface, in addition to DFT calculations we also use a Schottky-Mott⁶⁵ model to gain insight on the interface energetic level alignment. This model roughly predicts the height of the Schottky barrier, Φ_B , to be:

$$(5) \Phi_B = \Phi_{Pt} - \chi_{Fe_2O_3}$$

where Φ_{Pt} is the Pt work function and $\chi_{Fe_2O_3}$ is Fe_2O_3 's electron affinity. To obtain Φ_{Pt} we calculate the valence band edge position in a pure Pt (111) slab with respect to vacuum. $\chi_{Fe_2O_3}$ is evaluated by calculating the valence band edge in an oxygen terminated (0001) pure Fe_2O_3 slab with respect to vacuum and adding the band gap value calculated for the bulk material.

The Schottky barrier height can also be directly computed from the interface DOS by:

$$(6) \Phi_B = \mathcal{E}_C - \mathcal{E}_F$$

where \mathcal{E}_C is the Fe_2O_3 conduction band energy and \mathcal{E}_F is the Fermi energy in the interface.

III. Results and discussion

In this section, we introduce the results for the Pt(111)/ Fe_2O_3 (0001) interface in three sub-sections. First, we show the geometries for two different crystallographic orientation relationships. Second, we present the calculated interface energy of adhesion for each orientation and thereby determine which orientation is most stable. Finally, we present the electronic structure properties of the most stable interface orientation relationship and find that the effective mass of Fe_2O_3 is reduced upon Pt coverage.

1. Interface Geometries:

We considered two possible interface orientation relationships that have a minimal miss-fit as specified in the methods section (Figure 3). Our calculations show that the geometry of the S2 interface is preferred, in agreement with experiment.⁶⁶⁻⁶⁸ This is supported by several results: First, in the S2 interface all Pt atoms are bonded to O atoms, while in the S1 interface there are Pt atoms that are not bonded to Fe_2O_3 (seen in Figure 3d and 3b, respectively). Second, since the S2 interface has a smaller miss-fit, the bulk calculated geometries fit better with the experimental data (Table 1). Finally, the S1 interface has a longer Pt- Fe_2O_3 separation distance than the S2 interface (Table 1), suggesting the Pt is less strongly bonded to Fe_2O_3 in the S1 interface.

In addition, we notice Pt is affected more strongly than Fe₂O₃ by the lattice miss-match. This is expressed in the inter-planar distances, which are distorted more strongly in Pt than in Fe₂O₃ compared to the bulk structures by a factor of about two (Table 1). This can be attributed to the mechanical properties of each material. More specifically, in Pt the Poisson's ratio is 0.39,⁶⁹ while in Fe₂O₃ a value of about 0.2 was previously measured and calculated.^{70, 71} According to Poisson's ratio, planer stresses (due to lattice miss-fit) induce larger elongation of Pt at (111) planes spacing, in agreement with our results (Table 1). These geometrical distortions are smaller for the S2 interface.

Table 1 – Spacing of Pt (111) planes and Fe₂O₃ (0001) planes for bulk and interface structures.

	Pt-Pt: $d_{(111)}$ [Å]	O-O: $d_{(0001)}$ [Å]	Pt-O: $d_{(0001)-(111)}$ [Å]
Bulk - DFT+U	2.295	2.312	-
Bulk - Exp.	2.265 ⁷²	2.292 ⁷³	-
S1 Interface	2.438	2.247	2.008
S2 Interface	2.232	2.328	1.967

2. Energy of Adhesion:

To verify that the S2 interface is more favorable energetically we calculate the IEA for both interface structures. The IEA for the S2 interface is larger than that of the S1 interface for a given number of several Pt layers (Table 2). We conclude that the IEA of the S2 interface is $\gamma_{adh} \approx 2.85 \pm 0.1 \text{ J/m}^2$, and by extrapolating the values in Table 2 we expect that the IEA for S1 interface to be much smaller.

Table 2 – Adhesion energy with respect to varying number of Pt layers for the S1 and S2 interfaces.

Number of Pt layers	S1 Interface Energy of Adhesion [J/m ²]	S2 Interface Energy of Adhesion [J/m ²]
1	2.371	2.270
2	2.997	3.106
3	2.574	3.156
4	2.324	2.878
5	2.178	2.996
6	1.912	2.733
7	1.708	2.852

3. Electronic structure:

We now discuss the electronic structure of the stable S2 interface. There are several changes in the electronic structure of Fe₂O₃ under Pt coverage at the S2 interface: a continuum of states is formed in the gap, a Schottky barrier between the metal and metal-oxide emerges, there is reduction of effective mass in Fe₂O₃, the position of the last occupied state is shifted, and there are changes in the charge density distribution. Below we provide details.

3.1 Continuum of states

Upon addition of Pt metal over Fe₂O₃, instead of a band gap there is a continuum of states, even in the inner (non-interface) layers (Figure 4). The states involve hybridization of Pt 5d, Fe 3d, and O 2p states.

This strong hybridization was previously observed to much less extent in bulk Pt-doped Fe_2O_3 .⁴⁰ We suggest this continuum can cause interface recombination which is unwanted in photo-catalysis.^{74, 75}

3.2 Schottky barrier

Another disadvantage of metal coverage is the appearance of a Schottky barrier. A Schottky-Mott model⁶⁵ predicts $\Phi_B=0.71$ eV (obtained from Eq. 5 with $\Phi_{\text{Pt}}=5.62$ eV, $\chi_{\text{Fe}_2\text{O}_3}=6.63$ eV, valence band edge of Fe_2O_3 is 8.62 eV, and the band gap of Fe_2O_3 is 2.29 eV). However, calculating the Schottky barrier more accurately directly from the DOS (Eq. 6) gives a value of: $\Phi_B=1.1$ eV, which is more consistent with a model that considers pinning of the Fermi level around the mid gap,^{76, 77} such that the barrier is increased, and is roughly equal to half of the bulk band gap: $\Phi_B \approx E_g/2=1.14$ eV.

3.3 Reduction in effective mass

In addition, upon Pt coverage the effective charge carrier mass is favorably reduced in Fe_2O_3 . The bulk Fe_2O_3 conduction band DOS peak is sharp and abrupt due to the high localization of Fe 3d orbitals (Figure 4c). This causes a high electron effective mass previously calculated by us to be $3.98m_e$.⁴⁰ After Pt addition, Fe 3d conduction band states hybridize with Pt 5d states and have a wider distribution in energy. As a result there is a decrease in the abruptness of this peak (Figure 4b) and a smaller electron effective mass of $0.94m_e$. This is a conservative estimate, and in fact an upper limit for the new effective mass. Errors in this estimate (caused mostly by approximation of the exact energy where a rise in the conduction band DOS starts as shown in Appendix A) only lead to an even lower effective mass. The reduction in effective mass should increase conductivity in Fe_2O_3 , which is beneficial in catalytic systems.

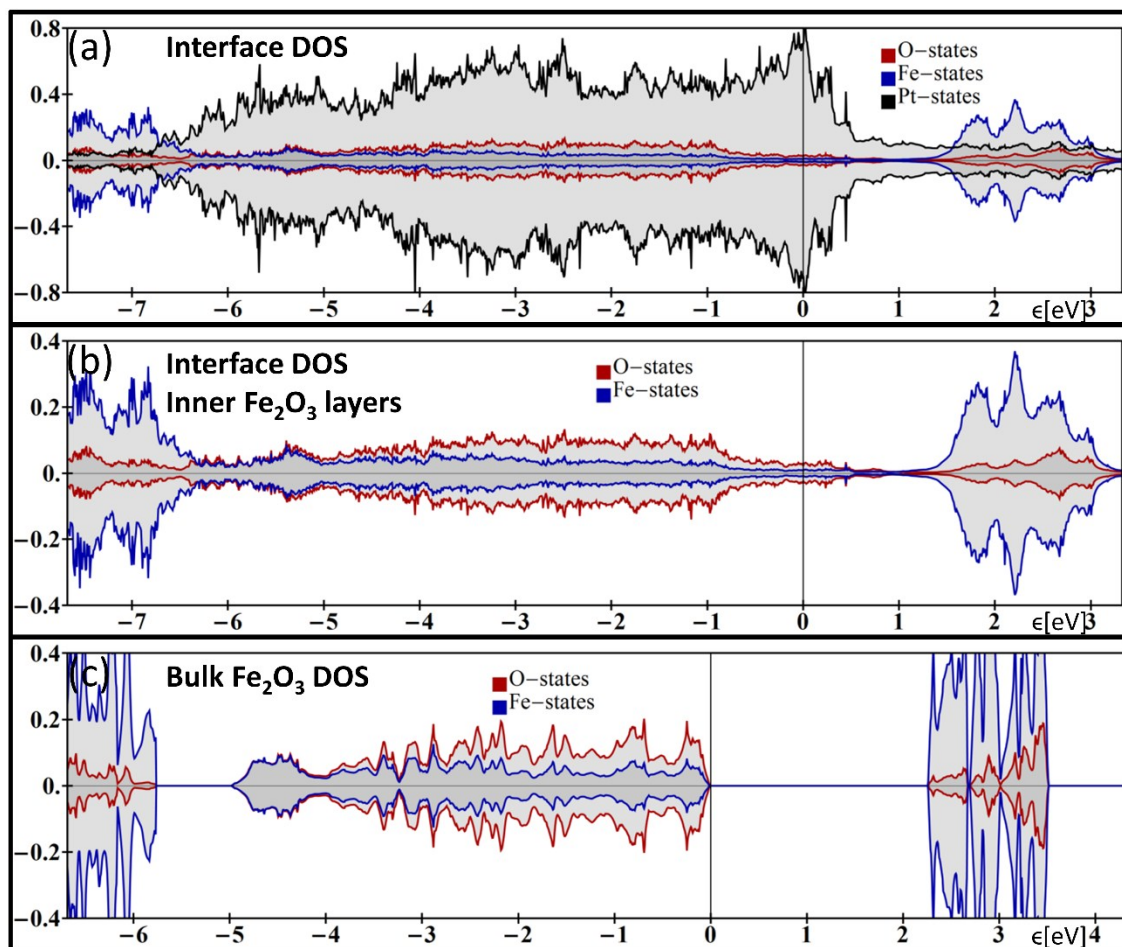


Figure 4 – Projected Density of States (PDOS) of the S2 interface: (a) the entire S2 interface, (b) the inner Fe_2O_3 layers from the S2 interface structure, and (c) bulk Fe_2O_3 . DOS is normalized to a maximum total density of one. The vertical line at zero is the last occupied orbital energy.

3.4 Shift in position of last occupied state

The last occupied state shifts towards the center of the gap (Figures 4a and 4c) of the metal-oxide upon Pt metal deposition. This shift can be explained by a change in band edge alignments. We calculate the valence band edge for the Pt(111) and $\text{Fe}_2\text{O}_3(0001)$ oxygen terminated surfaces to be: 5.62 and 8.62 eV. This is in agreement with experimental measurements of 6.10 eV⁷⁸ for Pt(111) and theoretical calculations with PW92+U ($U=4$ eV) of 8.58 eV for the $\text{Fe}_2\text{O}_3(0001)$ oxygen-terminated surface.⁵³ Since the valence band of Pt is higher than that of Fe_2O_3 , electrons transfer from Pt to Fe_2O_3 until equilibrium is reached, as reflected in the shift of the last occupied level.

3.5 Charge density distribution

The shift in the position of the last occupied state is confirmed by calculating the total number of electrons in each material with the charge density (Eq. 3) and comparing the charge density of the interface with that of the two pure material bare surfaces. We find that about two electrons (2.2e) are transferred from six Pt to six O atoms at the interface upon adhesion. This is further verified with a Bader charge analysis which reveals each interface O atom carries an additional 0.3e charge compared to the oxygen surface charge (0.6e Bader charge on each surface oxygen atom before Pt deposition), resulting in

a total of 1.8e gain in for all six surface oxygen atoms. This gain of electrons in the O atoms is apparent by loss of electrons in the Pt d_{z^2} orbitals perpendicular to the interface as can be observed in Figure 5a, and previously noted in Pt, Au, Pd, and Ru bilayers over Fe_2O_3 .²³ The excess of electrons in Fe_2O_3 could have a positive effect on transport at the interface.

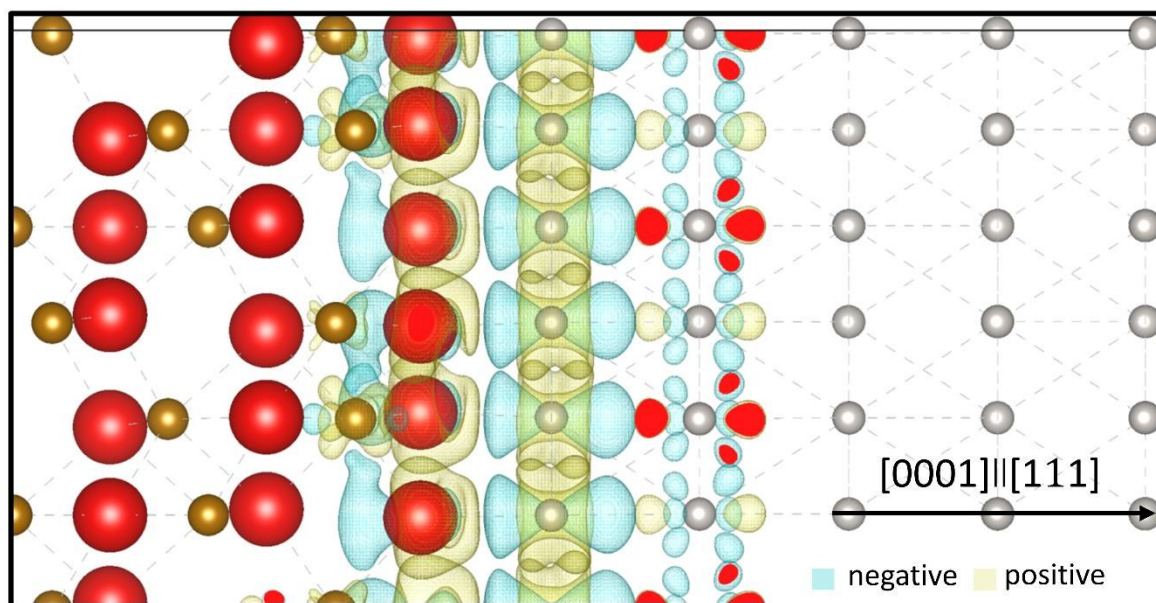


Figure 5 – Charge density difference plot between the S2 interface and corresponding Pt S2 and Fe_2O_3 S2 pure slabs fixed to similar geometry. Charge density contour is $\pm 6 \text{ m}\bar{e}/\text{\AA}^3$. Blue and yellow correspond to negative and positive contours, respectively, where negative is absence of electrons. Created with VESTA.⁵⁰

IV. Conclusions

We studied the Pt/ Fe_2O_3 interface at two different orientation relationships and find in agreement with experimental measurements⁶⁶⁻⁶⁸ that the $\text{Fe}_2\text{O}_3(0001)[1\bar{1}00]||\text{Pt}(111)[10\bar{1}]$ orientation is the most stable. Compared with the second interface orientation studied, this interface has a relatively large calculated adhesion energy of $\gamma_{adh} \approx 2.83 \pm 0.1 \text{ J/m}^2$, a high hexagonal symmetry, and long range atomic order. Therefore, this interface could be manufactured with less interfacial defects.

Upon covering Fe_2O_3 with Pt, Fe_2O_3 exhibits several electronic structure changes. The strong hybridization between Fe and Pt states causes a reduction of the electron effective mass in the metal-oxide from $3.98m_e$ to $0.94m_e$. This reduction could improve overall charge transport in a PEC cell and improve chemical reactions that couple charge transport. In addition, we calculate a large electronic charge relocating from the metal to the metal-oxide, which could have a positive influence on conductivity across the interface. These effects could be beneficial for catalysis over the Pt/ Fe_2O_3 interface, and since we calculate them at the interface we expect them to be most noticeable in ultrathin and nanoparticle sizes of Fe_2O_3 .

On the other hand, we find a continuum of states throughout the forbidden gap of Fe_2O_3 with Pt coverage. A continuum of surface states is likely to cause strong interface recombination. Furthermore, we find a Fermi level pinning with a Schottky barrier height of 1.1 eV for the Pt/ Fe_2O_3 junction. In order to overcome these issues, we suggest placing Pt as a back contact far from the electrolyte in a PEC cell. The external potential in a PEC will help electrons overcome the Schottky barrier. In addition, the

distance between Pt and the electrolyte will help the electrons avoid recombination with holes that accumulate near at the oxide/electrolyte interface during the water oxidation reaction.

We believe that these changes in the electronic structure of the oxide upon metal coverage also occur in other metal/oxide interfaces. We anticipate that understanding of how metal coverage changes the electronic structure of oxides will advance the development of future catalysts and electronic devices. For this purpose, our future work will focus on investigating more metal/oxide interfaces.

V. Acknowledgements

This research was supported by the Morantz Energy Research Fund, the Nancy and Stephen Grand Technion Energy Program, the I-CORE Program of the Planning and Budgeting Committee, and The Israel Science Foundation (Grant No. 152/11). O.N. acknowledges the Irwin and Joan Jacobs graduate school scholarship and the Leonard and Diane Sherman Interdisciplinary Graduate School Fellowship for excellence.

VI. Supporting Information Available

We provide relaxed geometries for the S1 and S2 pure Fe_2O_3 , pure Pt, and interface structures.

VII. Appendix A: Calculating effective mass reduction in the interface

The calculation of the effective mass in Pt-covered Fe_2O_3 from the DOS (fitting Eq. 4 by method of least squares) involves several steps. First, we must reduce the “background” states created by the interface. This is accomplished by using the Fe PDOS since the conduction band is comprised mostly of Fe 3d orbitals in Fe_2O_3 . Second, we set the conduction band edge value around the initial rise of DOS ± 0.3 eV since in the interface there is no obvious forbidden gap. Since the DOS effective mass is an estimate to the band diagram effective mass we only use the ratio obtained between pure and Pt-covered Fe_2O_3 and multiply this ratio by the value previously calculated (with a higher level of accuracy) to be $3.98m_e$ in pure Fe_2O_3 .⁴⁰ This results is the upper limit of $0.94m_e$ for the Pt-covered Fe_2O_3 (the least conservative estimate results in $0.27m_e$). As seen in Figure A.1, the DOS of Pt-covered Fe_2O_3 rises much less abruptly than in pure Fe_2O_3 .

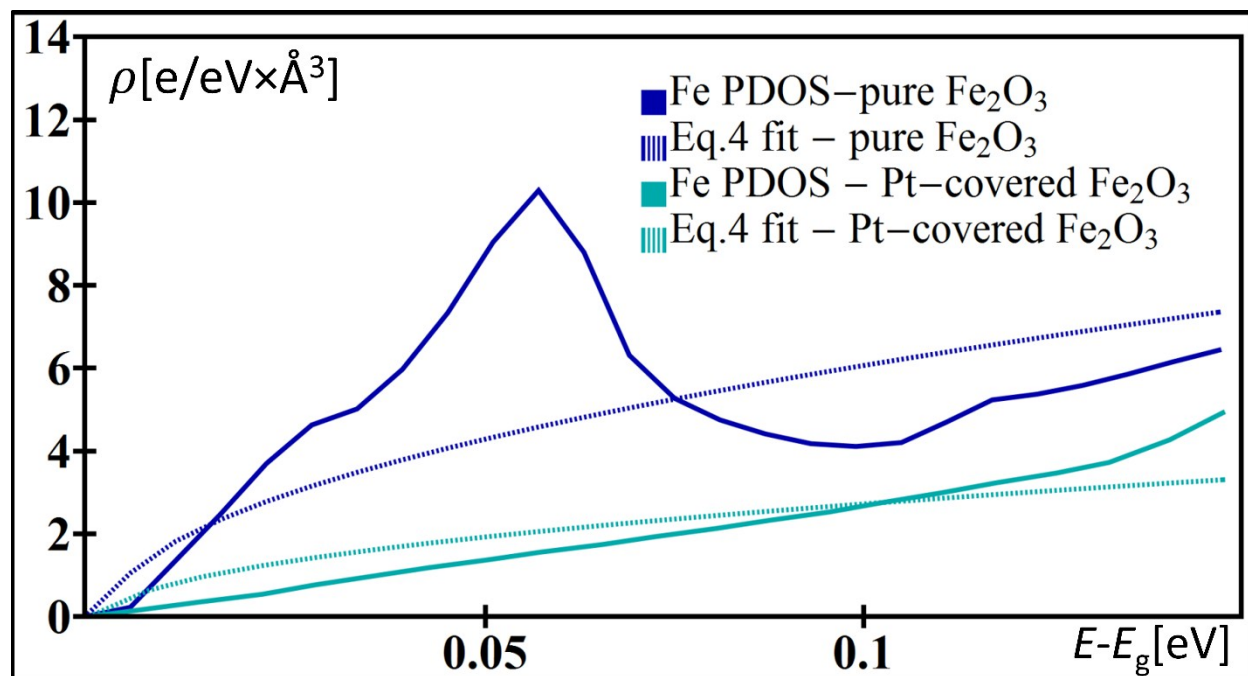


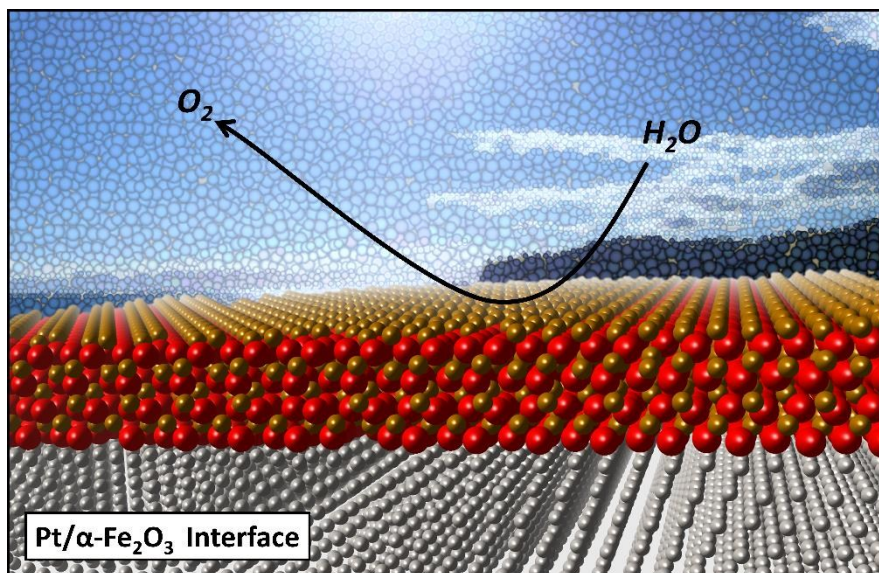
Figure A.1 – Fe PDOS in pure and Pt-covered Fe_2O_3 . Dashed lines are the fitted models according to Eq. 4. The x axis is energy such that zero is set to the band gap value. In Pt-covered Fe_2O_3 the background of surface states is deducted from the Fe PDOS.

VIII. References

1. I. H. Inoue, S. Yasuda, H. Akinaga and H. Takagi, *Physical Review B*, 2008, **77**, 035105.
2. S. J. Hwang, S. J. Yoo, S. Jang, T.-H. Lim, S. A. Hong and S.-K. Kim, *The Journal of Physical Chemistry C*, 2011, **115**, 2483-2488.
3. M. Haruta and M. Daté, *Applied Catalysis A: General*, 2001, **222**, 427-437.
4. G. C. Bond, C. Louis and D. T. Thompson, *Gold Bulletin*, 2006, **39**, 3.
5. H.-J. Freund and G. Pacchioni, *Chemical Society Reviews*, 2008, **37**, 2224-2242.
6. M. M. Schubert, S. Hackenberg, A. C. van Veen, M. Muhler, V. Plzak and R. J. Behm, *Journal of Catalysis*, 2001, **197**, 113-122.
7. W. Weiss and W. Ranke, *Progress in Surface Science*, 2002, **70**, 1-151.
8. A. Wongkaew and P. Limsuwan, *Advances in Chemical Engineering and Science*, 2013, **3**, 7.
9. N. Zhang, S. Liu, X. Fu and Y.-J. Xu, *The Journal of Physical Chemistry C*, 2011, **115**, 9136-9145.
10. K. Sivula, F. Le Formal and M. Grätzel, *ChemSusChem*, 2011, **4**, 432-449.
11. S. U. Khan, M. Al-Shahry and W. B. Ingler, *science*, 2002, **297**, 2243-2245.
12. P. Liao, J. A. Keith and E. A. Carter, *Journal of the American Chemical Society*, 2012, **134**, 13296-13309.
13. L. Steier, I. Herraiz-Cardona, S. Gimenez, F. Fabregat-Santiago, J. Bisquert, S. D. Tilley and M. Grätzel, *Advanced Functional Materials*, 2014, **24**, 7681-7688.
14. A. Basińska, T. P. Maniecki and W. K. Józwiak, *Reaction Kinetics and Catalysis Letters*, 2006, **89**, 319-324.
15. A. Basińska, W. Józwiak, J. Góralski and F. Domka, *Applied Catalysis A: General*, 2000, **190**, 107-115.
16. A. Basińska, L. Kępiński and F. Domka, *Applied Catalysis A: General*, 1999, **183**, 143-153.
17. M. Lewandowski, Y.-N. Sun, Z.-H. Qin, S. Shaikhutdinov and H.-J. Freund, *Applied Catalysis A: General*, 2011, **391**, 407-410.

18. B. Reddy and S. Khanna, *Physical review letters*, 2004, **93**, 068301.
19. W. Yan, S. M. Mahurin, B. Chen, S. H. Overbury and S. Dai, *The Journal of Physical Chemistry B*, 2005, **109**, 15489-15496.
20. Y. Wang, K. S. Chen, J. Mishler, S. C. Cho and X. C. Adroher, *Applied Energy*, 2011, **88**, 981-1007.
21. V. M. Dhavale and S. Kurungot, *The Journal of Physical Chemistry C*, 2012, **116**, 7318-7326.
22. P. Strasser, S. Koh, T. Anniyev, J. Greeley, K. More, C. Yu, Z. Liu, S. Kaya, D. Nordlund and H. Ogasawara, *Nature chemistry*, 2010, **2**, 454-460.
23. K. Wong, Q. H. Zeng and A. B. Yu, *The Journal of Physical Chemistry C*, 2011, **115**, 4656-4663.
24. Z. Zhang, M. F. Hossain, T. Miyazaki and T. Takahashi, *Environmental science & technology*, 2010, **44**, 4741-4746.
25. H. Dotan, O. Kfir, E. Sharlin, O. Blank, M. Gross, I. Dumchin, G. Ankonina and A. Rothschild, *Nat Mater*, 2013, **12**, 158-164.
26. E. Thimsen, F. Le Formal, M. Grätzel and S. C. Warren, *Nano letters*, 2010, **11**, 35-43.
27. O. Bengone, P. Blöchl, M. Alouani and J. Hugel, *Implementation of the Projector Augmented Wave LDA and U Method*, 2000.
28. G. Kresse and J. Hafner, *Physical Review B*, 1993, **47**, 558.
29. G. Kresse and J. Furthmüller, *Computational Materials Science*, 1996, **6**, 15-50.
30. S. Dudarev, G. Botton, S. Savrasov, C. Humphreys and A. Sutton, *Physical Review B*, 1998, **57**, 1505.
31. V. I. Anisimov, F. Aryasetiawan and A. Lichtenstein, *Journal of Physics: Condensed Matter*, 1997, **9**, 767.
32. L. Sandratskii, M. Uhl and J. Kübler, *Journal of Physics: Condensed Matter*, 1996, **8**, 983.
33. G. Rollmann, A. Rohrbach, P. Entel and J. Hafner, *Physical Review B*, 2004, **69**, 165107.
34. N. J. Mosey, P. Liao and E. A. Carter, *The Journal of chemical physics*, 2008, **129**, 014103.
35. L. Pauling and S. B. Hendricks, *Journal of the American Chemical Society*, 1925, **47**, 781-790.
36. L. W. Finger and R. M. Hazen, *Journal of Applied Physics*, 1980, **51**, 5362-5367.
37. A. Dianat, N. Seriani, M. Bobeth, W. Pompe and L. C. Ciacchi, *The Journal of Physical Chemistry C*, 2008, **112**, 13623-13628.
38. A. Kokalj and M. Causà, *Journal of Physics: Condensed Matter*, 1999, **11**, 7463.
39. R. K. Nomiya, M. J. Piotrowski and J. L. Da Silva, *Physical Review B*, 2011, **84**, 100101.
40. O. Neufeld and M. C. Toroker, *The Journal of Physical Chemistry C*, 2015, **119**, 5836-5847.
41. J. P. Perdew, K. Burke and M. Ernzerhof, *Physical review letters*, 1996, **77**, 3865.
42. P. E. Blöchl, *Physical Review B*, 1994, **50**, 17953.
43. G. Kresse and D. Joubert, *Physical Review B*, 1999, **59**, 1758.
44. P. E. Blöchl, O. Jepsen and O. K. Andersen, *Physical Review B*, 1994, **49**, 16223.
45. G. Lehmann and M. Taut, *physica status solidi (b)*, 1972, **54**, 469-477.
46. M. R. Hestenes and E. Stiefel, 1952.
47. G. Henkelman, A. Arnaldsson and H. Jónsson, *Computational Materials Science*, 2006, **36**, 354-360.
48. F. Morin, *Physical Review*, 1950, **78**, 819.
49. C. Searle and G. Dean, *Physical Review B*, 1970, **1**, 4337.
50. K. Momma and F. Izumi, *Journal of Applied Crystallography*, 2008, **41**, 653-658.
51. A. Kiejna and T. Pabisiak, *Journal of Physics: Condensed Matter*, 2012, **24**, 095003.
52. K. M. Young, B. M. Klahr, O. Zandi and T. W. Hamann, *Catalysis Science & Technology*, 2013, **3**, 1660-1671.
53. A. Kiejna and T. Pabisiak, *The Journal of Physical Chemistry C*, 2013, **117**, 24339-24344.
54. M.-T. Nguyen, S. Piccinin, N. Seriani and R. Gebauer, *ACS Catalysis*, 2014, **5**, 715-721.
55. M. C. Toroker, *The Journal of Physical Chemistry C*, 2014, **118**, 23162-23167.

56. C. Ophus, M. K. Santala, M. Asta and V. Radmilovic, *Journal of Physics: Condensed Matter*, 2013, **25**, 232202.
57. B. C. Bolding and E. A. Carter, *Molecular simulation*, 1992, **9**, 269-283.
58. L. I. Bendavid and E. A. Carter, *Surface Science*, 2013, **618**, 62-71.
59. G. Schlauzero and A. Pasquarello, *Diamond and Related Materials*, 2012, **23**, 178-183.
60. X.-G. Wang and J. R. Smith, *Physical review letters*, 2005, **95**, 156102.
61. O. Gritsenko and E. Baerends, *The Journal of chemical physics*, 2002, **117**, 9154-9159.
62. M. C. Toroker, D. K. Kanan, N. Alidoust, L. Y. Isseroff, P. Liao and E. A. Carter, *Physical Chemistry Chemical Physics*, 2011, **13**, 16644-16654.
63. W. Wunderlich, H. Ohta and K. Koumoto, *Physica B: Condensed Matter*, 2009, **404**, 2202-2212.
64. H. Peng and S. Lany, *Physical Review B*, 2012, **85**, 201202.
65. R. T. Tung, *Physical Review Letters*, 2000, **84**, 6078-6081.
66. W. Weiss and M. Ritter, *Physical Review B*, 1999, **59**, 5201.
67. A. Barbier, R. Belkhou, P. Ohresser, M. Gautier-Soyer, O. Bezenenet, M. Mulazzi, M.-J. Guittet and J.-B. Moussy, *Physical Review B*, 2005, **72**, 245423.
68. S. A. Chambers and T. Droubay, *Physical Review B*, 2001, **64**, 075410.
69. W. D. Callister and D. G. Rethwisch, *Materials science and engineering: an introduction*, Wiley New York, 7 edn., 2007, p. Appendix B, A.10.
70. M. Asada and Y. Omori, *Tetsu-To-Hagane/Journal of the Iron and Steel Institute of Japan*, 1983, **69**, 739-745.
71. D. Chicot, J. Mendoza, A. Zaoui, G. Louis, V. Lepingle, F. Roudet and J. Lesage, *Materials Chemistry and Physics*, 2011, **129**, 862-870.
72. *Joint Committee on Powder Diffraction Standards (JCPDS)*, card number 4-0802.
73. *Joint Committee on Powder Diffraction Standards (JCPDS)*, card number 33-664.
74. B. Klahr, S. Gimenez, F. Fabregat-Santiago, T. Hamann and J. Bisquert, *Journal of the American Chemical Society*, 2012, **134**, 4294-4302.
75. A. Duret and M. Grätzel, *The Journal of Physical Chemistry B*, 2005, **109**, 17184-17191.
76. A. Cowley and S. Sze, *Journal of Applied Physics*, 1965, **36**, 3212-3220.
77. C. A. Mead, *Solid-State Electronics*, 1966, **9**, 1023-1033.
78. G. Derry and Z. Ji-Zhong, *Physical Review B*, 1989, **39**, 1940.

Table of contents graphics

Solar water splitting may be improved by reduced charge carrier mass in Fe_2O_3 covered with Pt.